ELSEVIER

Journal of Fluids and Structures 22 (2006) 845–856

JOURNAL OF FLUIDS AND STRUCTURES

www.elsevier.com/locate/jfs

The effects of damping on the amplitude and frequency response of a freely vibrating cylinder in cross-flow

J.T. Klamo, A. Leonard*, A. Roshko

Graduate Aeronautics Laboratories, California Institute of Technology, 1200 E California Blvd, Pasadena, CA 91125, USA

Received 10 October 2005; accepted 20 April 2006
Available online 31 July 2006

Abstract

We have studied the effects of controlled damping on the amplitude and frequency response profiles of an elastically mounted cylinder in cross-flow. The dimensionless damping parameter, $b^* = 2b/\rho LDU$, which is closely related to the traditional "mass-damping" parameter, $m^*\zeta$, was varied over a wide range of values through the use of a variable magnetic eddy current damping system. For low damping *and* sufficiently high Reynolds number we observe the previously described large-amplitude, three-branch (initial, upper, lower) response profile, and for high damping or low Reynolds number we observe the small-amplitude, two-branch (initial and lower) response profile. However we find that, because of the influence of Reynolds number, the traditional labels of "high mass-damping" and "low mass-damping" are incomplete with regard to predicting a large or small-amplitude response profile. In our experiments, as damping is systematically increased, we observe a transition between these two profiles characterized by a gradual "erosion" and eventual disappearance of the large-amplitude section (upper branch) and the scaling down of the lower branch region. We find that jumps from the upper to the initial branch originate on the 2S/2P boundary in the Williamson–Roshko plane. Another new finding is a hysteresis between the lower branch and the desynchronized region, which only appears at low Reynolds numbers. We also explore changes in the frequency response profile, which are connected with the changes in the amplitude profile, for our upper branch cases. We observe that analogous to the three amplitude branches, there are three distinct branches for the frequency response.

Keywords: Vortex-induced vibrations; Damping; Reynolds number; Synchronization; Lock-in; Flow-induced oscillations

1. Introduction

Some early studies of vortex-induced vibrations (VIV) explored the effects of damping on the response behavior of the system. For instance, Vickery and Watkins (1964) reported peak amplitudes in air and water against a mass-damping parameter, and Scruton (1965) plotted the amplitude response profile of a dodecagonal cross-section model at three different damping values for a smooth surface and one for a rough surface. The most extensive damping study may have been done by Feng (1968) who explored the effects of damping on both the amplitude and frequency response for five different damping values. Feng used an electromagnetic eddy-current damper designed by Smith (1962) to impose controlled damping values on his system of circular and D-shaped cylinders. For the circular cylinder case, this

*Corresponding author. Tel.: +1 626 395 4465; fax: +1 626 577 9646.
E-mail address: tony@galcit.caltech.edu (A. Leonard).

0889-9746/$ - see front matter © 2006 Elsevier Ltd. All rights reserved.
doi:10.1016/j.jfluidstructs.2006.04.009

damping system allowed him to impose damping values in the range from $\zeta = 0.0010$ to 0.0032 (see Section 2 for parameter definitions). However, Feng's system had high mass-damping (due to the large m^* since his working fluid was air) and was constrained to the small-amplitude, two-branch response behavior. Due to this, he was only able to look at what effect a three-fold increase in damping has on a small-amplitude response profile.

More recent studies of damping effects on VIV have been largely directed toward low values of system damping and the high amplitudes that they allow. In most cases, the system damping is reported as a combined "mass-damping" parameter which lumps the damping coefficient with the system mass. Furthermore, these mass-damping effects have been investigated mainly around the maximum amplitude response of the system. A few recent studies have included systems with various damping values. For instance Khalak and Williamson (1997b) have full amplitude response curves of three different system masses, each exposed to four different damping values. However, as in the past, the range of damping values spanned was small and a change in system response was not seen, other than a slight decrease in maximum amplitude, because the main focus was to locate points in the "Griffin plot" [see, e.g., Skop and Griffin (1975) or Khalak and Williamson (1999)]. Another recent study by Hover et al. (1997) used a force-feedback controlled oscillation apparatus. During their study they tested four damping values ($\zeta = 0.000$, 0.001, 0.010, and 0.100) and reported total lift coefficient, phase angle, and amplitude response. Although they spanned a much larger range of ζ values than previous investigators, the amplitude response profile remained a large-amplitude response with slight changes until the highest damped case, which resulted in almost zero response.

In this paper we report on a systematic investigation on the effects of damping on the amplitude and frequency response profile for VIV of an elastically mounted cylinder. At least two types of system response are possible for VIV, as was reported by Khalak and Williamson (1997a). One of these involves a large-amplitude, three-branch response that was believed to result from low mass-damping. The other type of response is a small-amplitude response and involves only a two-branch profile, consisting of the initial and lower branch, and is believed to correspond to high mass-damping. Also, consistent with Khalak and Williamson (1997a), we denote the region beyond the lower branch in which there are high tunnel speeds and little amplitude response as the desynchronized region. We observe the large-amplitude, three-branch response and the small-amplitude, two-branch response and investigate the transition between them, as damping is varied, using a variable magnetic eddy-current (VMEC) damping system. The corresponding frequency response during this transition is equally as important and is also studied. Although not emphasized and often not considered by previous investigators, Reynolds number also plays an important role in the type of response that one sees, in that the response is controlled by not only system damping but by Reynolds number as well.

2. Theoretical development

Consider a mass–damper–spring system with mass m, damping b, and elasticity k. Of interest is the response behavior of the system, characterized by the nondimensional response amplitude, $A^* = A/D$, and frequency, $\omega^* = \omega D/U = 2\pi f^*$, where D is the cylinder diameter and U is the free-stream velocity. For such an arrangement, one can obtain [see Shiels et al. (2001) for details] a nondimensional governing equation of motion for $y^* = y/D$ as follows:

$$m^*\ddot{y}^* + b^*\dot{y}^* + k^*y^* = C_L(t^*), \tag{1}$$

where all quantities are made nondimensional using the fluid properties, free-stream velocity, and cylinder diameter and length [the nondimensional quantities are defined in detail in Klamo et al. (2005)]. Note that the damping, b^*, is related to the traditional damping parameter, ζ, by $b^* = (2/U_R)\,m^*\zeta$, where $U_R = U/(\omega_N D)$, $\zeta = b/(2\sqrt{km})$ and ω_N is the natural frequency of the system in air, U_R is the reduced velocity.

For a cylinder with minimal end effects that is allowed to oscillate normal to the flow direction, we expect a functional dependence on the amplitude and frequency response,

$$\begin{aligned} A^* &= A^*(m^*, b^*, k^*, \mathrm{Re}),\\ \omega^* &= \omega^*(m^*, b^*, k^*, \mathrm{Re}), \end{aligned} \tag{2}$$

where Re is the Reynolds number of the cylinder. If one assumes sinusoidal motion to a first approximation, then the mass and stiffness of the system can be combined into a single parameter, k^*_{eff}, the effective stiffness of the system defined as $k^*_{\mathrm{eff}} = -\omega^{*2}m^* + k^*$. This potentially simplifies the response behavior as follows:

$$\begin{aligned} A^* &= A^*(k^*_{\mathrm{eff}}, b^*, \mathrm{Re}),\\ \omega^* &= \omega^*(k^*_{\mathrm{eff}}, b^*, \mathrm{Re}), \end{aligned} \tag{3}$$

and reduces the parameter space since m^* and k^* are combined and replaced by the effective stiffness parameter, whereas in the traditional formulation there are four independent parameters (U_R, ζ, m^*, Re).

3. Experimental details

All experiments were conducted in a free-surface low-speed water tunnel facility with test-section dimensions of 45.7 cm wide by 58.4 cm deep. A mass–damper–spring system was placed on top of the water tunnel test section and the circular cylinders were attached to this system and suspended downward into the tunnel. This arrangement can be seen in Fig. 1. The system consists of a pair of air-bearings to which a mounting plate and cylinder is attached. The motion of the cylinder and plate is recorded using a LVDT. These air-bearings restrict the motion of the cylinder and plate to be in the transverse direction to the flow while also providing extremely low inherent damping. Thin stainless-steel plates can be attached to the mounting plate to vary the system mass as desired. The attachment points for the springs can handle multiple springs in a vertical parallel arrangement so that any desired stiffness can be achieved. The springs were hand-made from long coils of metal so that the stiffness and length could be controlled.

The main innovation in this study was the construction of a VMEC damping system. The VMEC damping system can be seen in detail in Fig. 1 and consists of six electromagnets and a copper conducting plate. The six electromagnets are identical to each other and made of 1″ (2.54 cm) diameter 1018 steel wrapped in 18 gauge magnet wire. These magnets are attached to aluminum plates that are then in turn attached to the base of the test apparatus. The conducting plate is copper alloy 110 with a thickness of 1/32″ (0.08 cm) and is attached to the mounting plate so that it moves in unison with the cylinder and mounting plate. Thus, the conductive plate oscillates between the pairs of electromagnets. The system is activated by using a Kepco power supply with current control to supply the desired current to the magnet wires. This current induces a magnetic field which is amplified by the iron in the steel rods. In order to generate any useful damping, and especially to generate the high damping values needed for this study, a strong magnetic field needed to be generated. Since the apparatus is space-limited as well as power-supply-limited, the steel rods could not simply be wrapped with an enormous number of coils (magnetic field strength is proportional to number of coils). Instead, large currents were supplied to the electromagnets (for certain tests around 1 A).

For this study, four different system configurations were used. The parameters for each system can be found in Table 1. During the course of each test, the water temperature was $20 \pm 1\,^{\circ}\mathrm{C}$, corresponding to a kinematic viscosity of

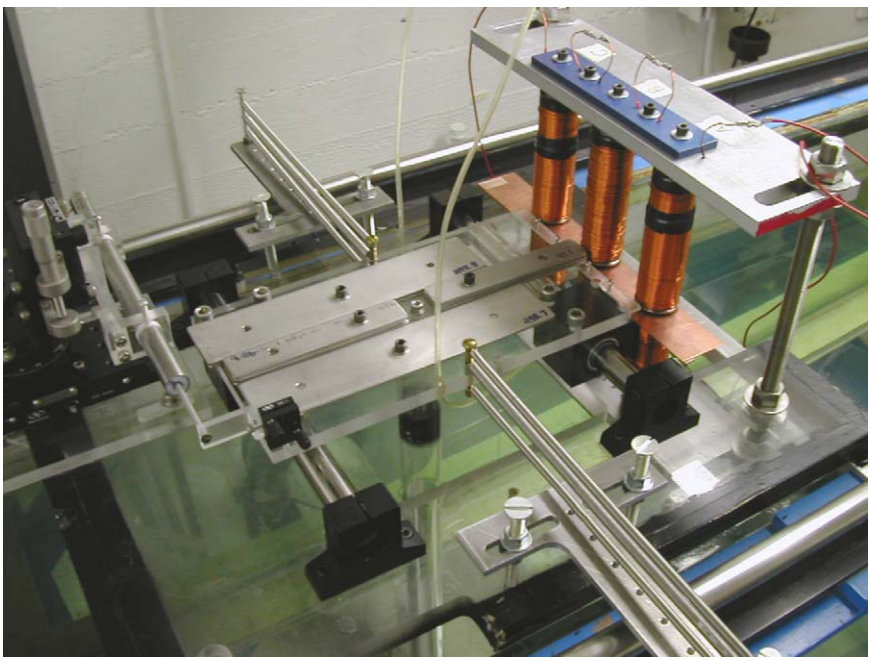

Fig. 1. Experimental test stand showing the mass–damper–spring system comprising the air bearings, mounting plate, cylinder, stainless-steel plates, springs, copper conducting plate, and electromagnets. Cylinder displacements are measured using a LVDT.

Table 1
System configuration for each test sequence

Sequence	Mass (kg)	m^*	Damping range (kg/s)	Stiffness (N/m)	Cylinder diameter (mm)	Reynolds number at A^*_{max}
1	1.85	78.3	0.018–0.278	65.5	10.0	525
2	3.70	156.7	0.023–0.263	135.0	10.0	525
3	1.85	78.3	0.027–0.537	260.0	10.0	1000
4	2.39	7.1	0.016–0.977	13.5	37.8	2600

$1.004 \times 10^{-6} \pm 0.030 \times 10^{-6}\,m^2/s$. This resulted in variations in Reynolds number during tests ranging from $Re|_{A^*_{max}} \sim 525 \pm 15$ to $Re|_{A^*_{max}} \sim 2600 \pm 75$. All the cylinders had a wetted length, L, of approximately 47 cm so that we only consider high aspect ratio systems $L/D > 10$ with minimal end effects.

Due to the various nondimensional parameters that researchers use for the study of VIV, we give some of the system parameters in Table 1 in dimensional form so that they can be converted to the formulation that each researcher chooses. Finally, since most nondimensional variables, such as b^* and Re, change values during the course of a test run, we use the notation of a subscripted "A^*_{max}" after the variable name, such as $b^*|_{A^*_{max}}$ or $Re|_{A^*_{max}}$, to refer to the value of that nondimensional quantity at the maximum amplitude point, A^*_{max}, for that given test.

4. Experimental procedure

For a given system with certain m, b, k, and D values, a test *Run* was completed by spanning the range of velocities of interest four times, twice in increasing and twice in decreasing increments. This was done to look for hysteresis effects and to gauge repeatability. As U is varied all nondimensional parameters except m^* will vary. However, as long as $k > 0$, all values of k^*_{eff} of interest will be spanned by such a test run. This procedure was then repeated multiple times on the same system but with different values of damping. These repeated test runs at various b values then encompass a test *Sequence*.

Although each point that is part of a given test run corresponds to a different tunnel speed and thus a different Reynolds number and b^* value, each value of k^*_{eff} within a test sequence (except k^*_{eff} slightly less than 0) corresponds to nearly the same tunnel speed and Reynolds number for those points. Therefore, the differences in a test sequence are essentially damping effects only.

5. Experimental results

First, Sequence 3 ($Re|_{A^*_{max}} \sim 1000$) will be used to show in Section 5.1 how a given system transitions from a large-amplitude response profile to a small-amplitude response profile. Since one of the dramatic changes in the amplitude response involves the scaling down of the lower branch, this will be explored in Section 5.2 using selected runs from Sequence 3. Next, upper branch cases (defined here as those systems which have a low enough damping and sufficiently high Reynolds number to allow for an upper branch) will be used to examine the "erosion" of the upper branch portion of the amplitude response, Section 5.3, and the corresponding changes in the frequency response, Section 5.4. The transition from the lower branch to a desynchronized state and its dependence on increasing or decreasing tunnel speeds is discussed in Section 5.5. Finally, Section 5.6 explores the coupling between damping and Reynolds number in VIV response behavior.

5.1. Large-amplitude profile to small-amplitude profile transition

The transition undertaken by a system in going from a large-amplitude, three-branch response, to a small-amplitude, two-branch response can be seen in Fig. 2(a) using the traditional reduced velocity formulation. The damping values for Sequence 3 can be found in Table 2. The most lightly damped case, Run 3(a), shows the expected low mass-damping, three-branch response. It contains an initial, upper, and lower branch as pointed out by Khalak and Williamson (1997a). The highest damped case, Run 3(j), shows the expected high mass-damping, two-branch response. It contains only an initial and lower branch and is similar, although not identical, to the response seen by Feng (1968). Runs 3(c)–3(g) show how the system transitions between these two very different system responses. The two most dramatic changes are the scaling down of the lower branch portion and the "erosion" and eventual disappearance of the upper branch, or large-amplitude, portion of the response.

These same results are shown in Fig. 2(b) using the effective stiffness parameter. It is important to note that in general, effective stiffness decreases as flow velocity increases, for a given system. Therefore, for convenience in

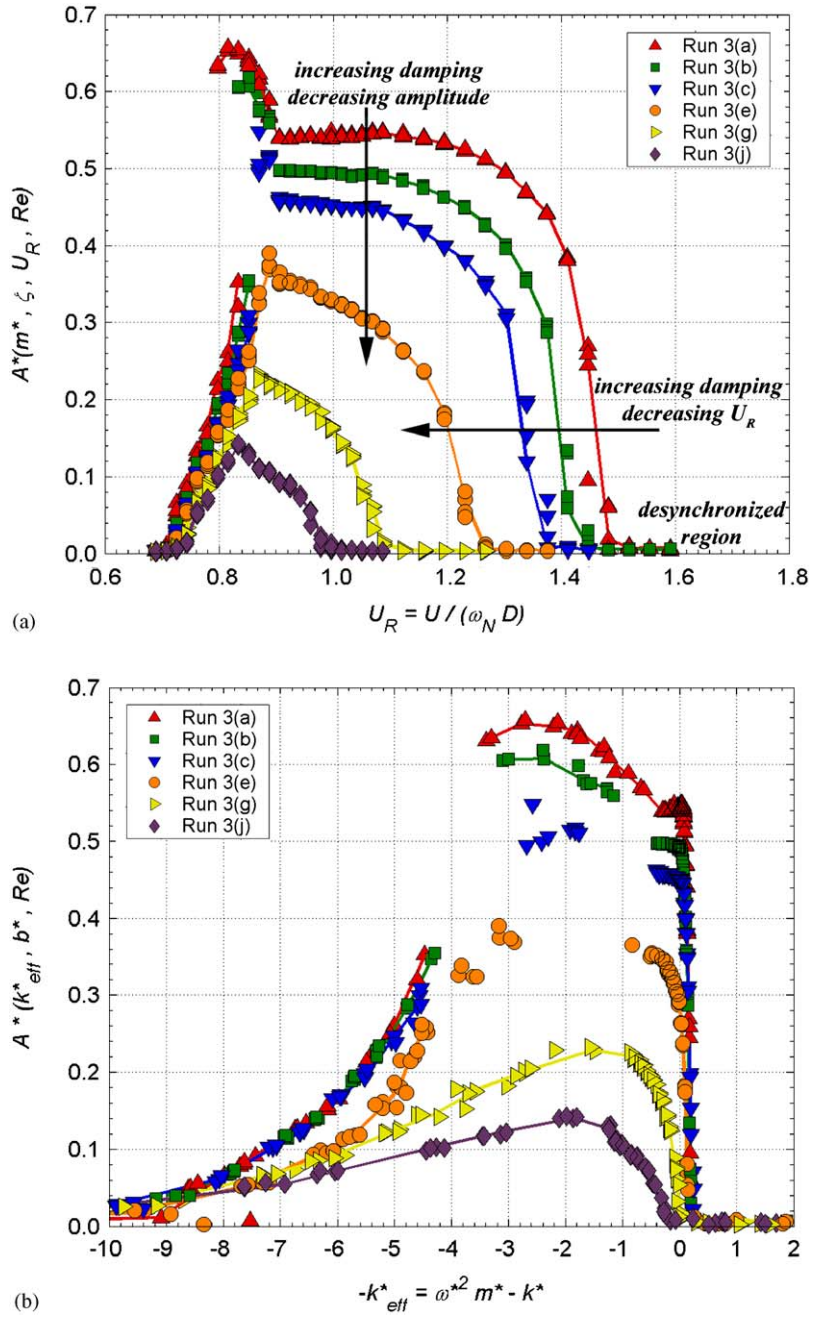

Fig. 2. Sample of Sequence 3 amplitude response profiles in two formulations: (a) in the traditional formulation; the two effects that cause the scaling down of the lower branch as damping is increased are also shown and (b) in the effective stiffness formulation.

comparing with the traditional plot in Fig. 2(a), we present plots against negative effective stiffness, $-k^*_{\text{eff}} = \omega^{*2} m^* — k^*$, since this increases with increasing U^*.

5.2. Scaling down of the lower branch

The scaling down of the lower branch is due to two factors, both of which can be seen by looking at the lower branches in Fig. 2(a). First, the value of A^* decreases, for a given U_R, as damping is increased. This trend is shown by

Table 2
Damping values for all Sequence 3 test runs

Run	ζ	$b^*\|_{A^*_{\max}}$
3(a)	0.0006	0.12
3(b)	0.0015	0.28
3(c)	0.0026	0.46
3(d)	0.0038	0.67
3(e)	0.0051	0.90
3(f)	0.0071	1.26
3(g)	0.0085	1.54
3(h)	0.0100	1.85
3(i)	0.0109	1.99
3(j)	0.0122	2.29

the vertical arrow in Fig. 2(a). Notice the diminishing amplitudes of the nearly constant-amplitude portion of the lower branch ($0.90 < U_R < 1.1$ for upper branch cases with these system parameters). For the most lightly damped case, the lower-branch constant-amplitude portion is approximately $A^* \sim 0.54$ and, as damping is increased, it steadily goes down $A^* \sim 0.50$ [Run 3(b)] and $A^* \sim 0.46$ [Run 3(c)].

Second, as damping is increased, the reduced velocity value that corresponds to the system entering the desynchronized region decreases. This trend is shown by the horizontal arrow in Fig. 2(a). For instance, for the most lightly damped case, the desynchronized region is entered at a $U_R \sim 1.50$ and as damping is increased, this region is entered sooner, $U_R \sim 1.25$ [Run 3(e)] and $U_R \sim 1.00$ [Run 3(j)].

5.3. Erosion of the upper branch: amplitude study

As can be seen in Fig. 2(a) and (b), part of the transition from a large-amplitude response to a small-amplitude response involves the disappearance of the upper branch portion of the profile. This disappearance is a gradual process that occurs over a range of damping values. Because the upper branch is located near a hysteretic region, that has been noted by several investigators, including Feng (1968), Brika and Laneville (1993), and Khalak and Williamson (1999), the erosion of the upper branch is associated with two effects. One occurs for increasing tunnel speeds and one for decreasing tunnel speeds. This erosion of the upper branch can be seen in Fig. 3, in the traditional reduced velocity formulation, containing the four most lightly damped cases from Sequence 3.

An important point to notice is that the *upper* branch meets the *lower* branch at a *fixed* value of U_R, independent of damping. For this particular system it occurs at $U_R \sim 0.90$ (see Fig. 3); for other systems the value is different but always independent of damping. The first effect that controls the existence and size of the upper branch is the point at which the jump from the *initial* to the *upper* branch occurs for increasing tunnel speeds (solid lines in Fig. 3). As damping is increased the size of the upper branch decreases due to the fact that the jump to the upper branch is delayed. This can be seen in Fig. 3 as a higher reduced velocity value at which the amplitude jump discontinuity occurs. For Run 3(a), the jump occurs around $U_R \sim 0.84$, whereas for Run 3(d) it occurs around $U_R \sim 0.88$. Since the ending of the upper branch is fixed at $U_R \sim 0.90$, as the jump to the upper branch keeps occurring at higher and higher reduced velocity values, the size of the upper branch decreases.

The second effect that controls the existence and size of the upper branch is the point where the jump downward from *upper* to *initial* branch occurs (dashed lines in Fig. 3). As damping is increased, this point occurs at higher values of U_R. In Fig. 3, for Run 3(a), it occurs around $U_R \sim 0.80$ whereas for Run 3(b), the jump downward occurs around $U_R \sim 0.83$. The jump downward from upper to initial branch, as tunnel velocity is decreased, appears to coincide with regimes of the Williamson-Roshko (1988) plane (henceforth WR plane), which describes the type of vortex shedding that can occur, based on the frequency and amplitude of the oscillating cylinder. The jump downward in Fig. 4 occurs when the boundary between the 2S and the 2P regimes is reached. [In this notation, 2S denotes two vortices shed per oscillation period and 2P denotes 2 pairs (4 vortices) per period. Note that the independent variable is now $1/f^*$.] The damping values for select runs of Sequence 2 can be found in Table 3 and for each run of Sequence 4 in Table 4. It was noted by Khalak and Williamson (1999) that the jump between initial and upper branch corresponds to a change in the WR plane between a 2S and a 2P wake structures. More specifically, we observe that when tunnel velocity is decreased, the

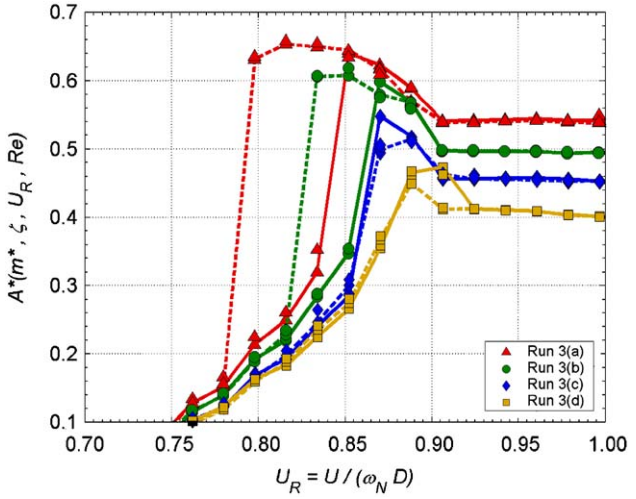

Fig. 3. Erosion of the upper branch for Sequence 3. Solid lines represent increasing tunnel speeds and dashed lines represent decreasing tunnel speeds.

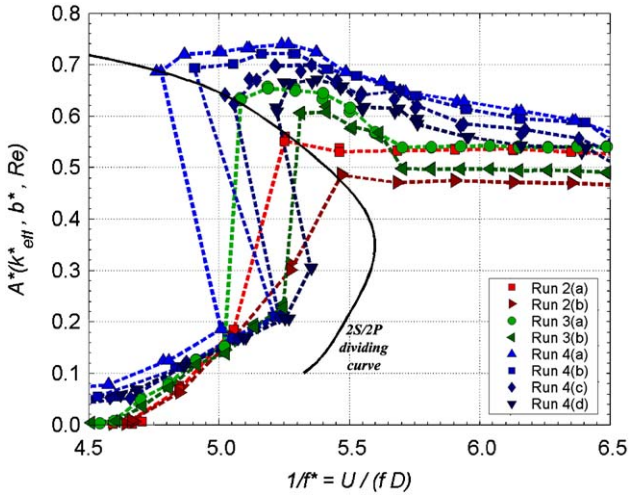

Fig. 4. Jump downward from the upper branch to initial branch and the 2S/2P dividing curve in the Williamson–Roshko plane. Shown are selected runs from Sequences 2–4.

jump downward occurs when the amplitude response reaches the 2S/2P boundary. Because of the negative slope of this dividing line and the fact that an increase of damping decreases the overall response amplitude, this line is crossed at higher values of reduced velocity, U_R, as damping is increased. Ultimately by this process the upper branch disappears for decreasing tunnel speed runs. We observe the same phenomenon for Sequence 4 ($\mathrm{Re}|_{A^*_{\max}} \sim 2600$) and Sequence 2 ($\mathrm{Re}|_{A^*_{\max}} \sim 525$), as seen in Fig. 4. On the other hand, we observe that as tunnel velocity is increased the system jumps to various locations in the 2P regime, apparently dependent on both Reynolds number and damping.

5.4. Erosion of the upper branch: frequency study

The corresponding changes in frequency, as the upper branch amplitude profile is being eroded away, are shown in the effective stiffness formulation in Fig. 5(a). In the figure, increasing tunnel speed data is shown using solid lines and

Table 3
Damping values for select Sequence 2 test runs

Run	ζ	$b^*\|_{A^*_{max}}$
2(a)	0.0005	0.19
2(b)	0.0011	0.39

Table 4
Damping values for all Sequence 4 test runs

Run	ζ	$b^*\|_{A^*_{max}}$
4(a)	0.0014	0.03
4(b)	0.0055	0.10
4(c)	0.0107	0.20
4(d)	0.0160	0.30
4(e)	0.0211	0.39
4(f)	0.0274	0.50
4(g)	0.0410	0.73

decreasing tunnel speed data is shown using dashed lines. The frequency response for these upper branch cases exists along three branches. Branch 1 frequencies correspond to initial branch amplitudes, branch 2 frequencies to upper branch amplitudes, and branch 3 frequencies to lower branch amplitudes. As damping is increased, three changes in the frequency response take place. First, the jump from branch 1 to branch 2 is delayed and occurs at a slightly smaller effective stiffness value. Second, the slope of the roughly linear branch 2 decreases. Lastly, the size of the hysteresis, the difference between the solid and dashed lines, decreases. These three changes are displayed in simplified form in the schematic of Fig. 6, which is representative of the *general* trend. For example, these same three changes can be seen in Fig. 5(b) which is the frequency response profile for the upper branch cases in Sequence 4. However, it can be seen that the *details* of the actual response profiles, the slopes of the branches and the actual frequency and effective stiffness values at the beginning and end of the branches, do depend on Reynolds number. This can easily be seen by noticing the differences between Fig. 5(a) and (b). Perhaps one of the most obvious differences is the jump between branches 1 and 2. In Fig. 5(a) (Sequence 3) the jump has a slightly negative slope whereas in Fig. 5(b) (Sequence 4) the jump has a large positive slope.

5.5. Hysteresis between lower branch to desynchronized region

Many researchers have investigated the hysteretic jump between the initial and upper branches and the intermittent switching between the upper and lower branches (Khalak and Williamson, 1999). However, except for some recent results by Singh and Mittal (2005) on a flexibily mounted cylinder, there has been very little discussion on the transition from the lower branch to the desynchronization region. Our results show that not only is there a hysteretic jump between the lower branch and the desynchronization region, but also that the size of this hysteresis is damping dependent. This new result can be seen in Fig. 7 below in the reduced velocity formulation. The damping values for Sequence 1 can be found in Table 5. In this figure, the solid lines represent the system going from the lower branch to the desynchronization region as tunnel speed is increased and the dashed lines represent the system going from a desynchronized state to the lower branch as speed is decreased. As can be seen in Fig. 7 for Sequence 1, the reduced velocity value at which the system changes between the lower branch and a desynchronized state depends on whether the tunnel speed is increasing or decreasing. Another interesting result is that, unlike the increasing tunnel speed case, where the amplitude slowly decreases for each test point until the desynchronized region is reached in a fairly smooth manner, for the decreasing velocity case the change from desynchronized region to lower branch is dramatic and takes the form of a jump discontinuity.

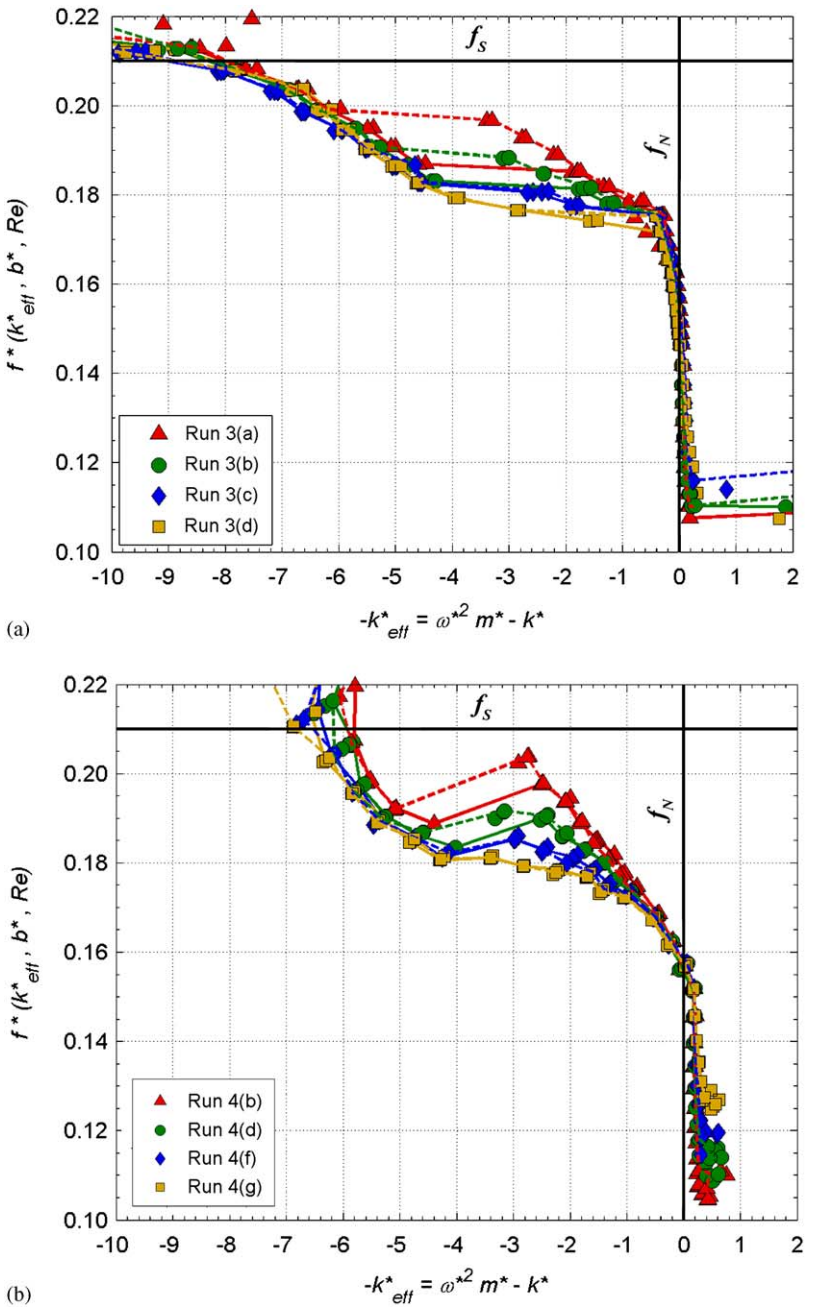

Fig. 5. Effects of damping on the frequency response profiles for two different upper branch cases using the effective stiffness formulation. Solid lines represent increasing tunnel speeds and dashed lines represent decreasing tunnel speeds. f_S: stationary cylinder Strouhal frequency; f_N: system natural frequency in air. (a) Sequence 3 frequency responses. (b) Sequence 4 frequency responses.

The size of these hysteretic jumps depends on the level of damping in the system. In general, as damping is increased, the width of the hysteretic jump decreases. This can be seen by noting the large hysteretic jumps for the most lightly damped cases, Runs 1(a)–1(c), the smaller width as damping is increased for Run 1(e), and finally, in the most heavily damped system, Run 1(g), the width of the hysteresis is only a single test point. It is difficult to assign single reduced velocity values for where these hysteretic jumps will occur, since they appear to be sensitive to factors such as slight

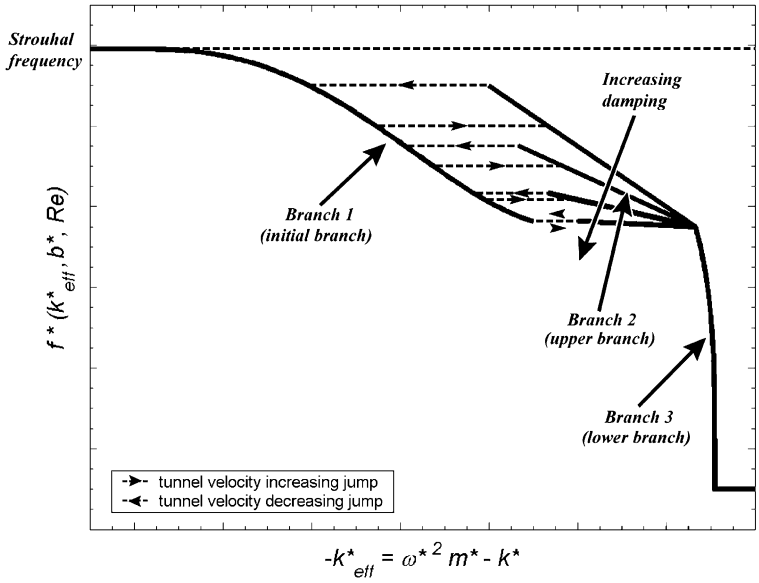

Fig. 6. Schematic showing the general trend of damping effects on the frequency response profiles for upper branch cases.

perturbations in the flow. This is not to say that the existence itself is sensitive, for the presence of these hysteretic jumps is always observed in repeated tests. However, the reduced velocity values at which the jumps occur does vary during identical repeated tests.

Perhaps one reason that the lower branch to desynchronized region hysteresis has been missed is the fact that it appears to be a low Reynolds number effect. We found that our $\mathrm{Re}|_{A^*_{\max}} \sim 2600$ (Sequence 4) displayed no hysteresis and $\mathrm{Re}|_{A^*_{\max}} \sim 1000$ (Sequence 3) displayed hysteresis only on the two most lightly damped cases. However, both of our $\mathrm{Re}|_{A^*_{\max}} \sim 525$ tests showed this hysteresis prominently.

5.6. Effects of Reynolds number

Many of the damping effects discussed here have Reynolds number effects as well. Some of these are discussed in more detail in Klamo et al. (2005). Since damping and Reynolds number are both at play, depending on the Reynolds number and damping range that one is investigating, the effects may not be exhibited. For example, it was found that for Sequences 1 and 2, no true upper branch response existed, for any of the damping values tested. Thus, for a given b^* we observe an upper branch at higher Reynolds number [see Fig. 2(a) Run 3(a)] but it is not present at low Reynolds number [see Fig. 7 Run 1(a)]. That is, the upper branch response is not simply dependent on damping. In order to have an upper branch response, one needs a low damping value *and* a high enough Reynolds number. The response profile of the system is controlled by the combination of damping and Reynolds number.

6. Conclusions

Khalak and Williamson (1997a) classified the amplitude response of a freely vibrating cylinder in cross-flow as a large-amplitude, three-branch response at low mass-damping and a small-amplitude, two-branch response at high mass-damping. In the present investigation, we have shown how a given system transitions between these two classifications as damping is varied. We observe that a mass-damping parameter is insufficient to define the classification; the Reynolds number also has an important effect. Low damping *and* high Reynolds number are necessary for the upper branch to exist. We find that for decreasing tunnel speeds, the jump downward from upper to initial branch is controlled by the dividing 2S/2P curve in the Williamson–Roshko plane. In addition to the well-known hysteresis jump between the initial and upper branches of the three-branch response, we find another hysteresis in the transition from the lower branch to the desynchronized region. This hysteresis exists for low Reynolds numbers and is

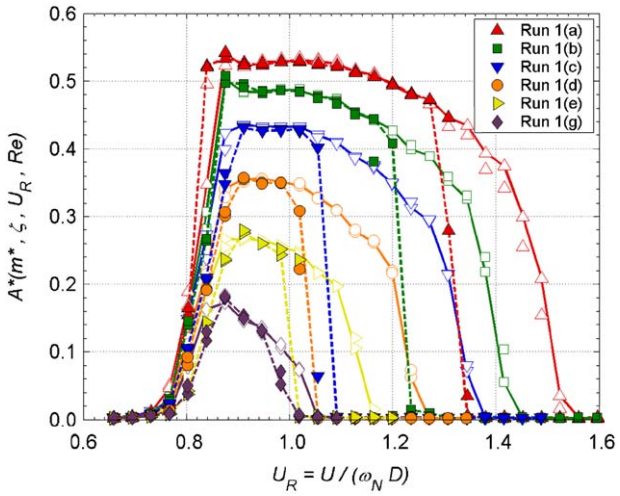

Fig. 7. Amplitude response profiles for Sequence 1 showing the lower branch to desynchronized region hysteresis. Solid lines and white data-points show increasing tunnel speeds and dashed lines and colored data-points show decreasing tunnel speeds.

Table 5
Damping values for all Sequence 1 test runs

Run	ζ	$b^*\|_{A^*_{\max}}$
1(a)	0.0008	0.15
1(b)	0.0016	0.29
1(c)	0.0028	0.49
1(d)	0.0042	0.73
1(e)	0.0056	0.98
1(f)	0.0070	1.24

not observed in $\mathrm{Re}|_{A^*_{\max}}$ experiments greater than around $\mathcal{O}(10^3)$. Furthermore, we describe the effects of damping and Reynolds number on this hysteresis. We also describe the damping and Reynolds number effects on the corresponding frequency response for upper branch cases.

Acknowledgements

The application of magnetic damping described here was inspired by the theses of J. D. Smith and C. C. Feng who were students of Geoffrey V. Parkinson, recently deceased. We dedicate this paper to Geoff. We would like to thank Prof. Morteza Gharib for his continued involvement in this research effort and Prof. David Goodwin for his helpful suggestions regarding the damping system. We gratefully acknowledge the financial support provided by ONR Grant # N00014-94-1-0793. Scholarship support was provided by the National Science Foundation graduate fellowship program.

References

Brika, D., Laneville, A., 1993. Vortex-induced vibrations of a long flexible circular cylinder. Journal of Fluid Mechanics 250, 481–508.
Feng, C.C., 1968. The measurement of vortex induced effects in flow past stationary and oscillating circular and D-section cylinders. M.A. Sc. Thesis, University of British Columbia, Vancouver, Canada.
Hover, F., Miller, S.N., Triantafyllou, M.S., 1997. Vortex-induced vibration of marine cables: experiments using force feedback. Journal of Fluids and Structures 11, 307–326.

Khalak, A., Williamson, C.H.K., 1997a. Fluid forces and dynamics of a hydroeleastic structure with very low mass and damping. Journal of Fluids and Structures 11, 973–982.

Khalak, A., Williamson, C.H.K., 1997b. Investigation of relative effects of mass and damping in vortex-induced vibration of a circular cylinder. Journal of Wind Engineering and Industrial Aerodynamics 69-71, 341–350.

Khalak, A., Williamson, C.H.K., 1999. Motions, forces and mode transitions in vortex-induced vibrations at low mass-damping. Journal of Fluids and Structures 13, 813–851.

Klamo, J.T., Leonard, A., Roshko, A., 2005. On the maximum amplitude for a freely vibrating cylinder in cross-flow. Journal of Fluids and Structures 21, 429–434.

Scruton, C., 1965. On the wind-excited oscillations of stacks, towers and masts. In: Proceedings Symposium on Wind Effects on Buildings and Structures. HMSO, London, pp. 798–836 Paper 16.

Shiels, D., Leonard, A., Roshko, A., 2001. Flow-induced vibration of a circular cylinder at limiting structural parameters. Journal of Fluids and Structures 15, 3–21.

Singh, S.P., Mittal, S., 2005. Vortex-induced oscillations at low Reynolds numbers: hysteresis and vortex-shedding modes. Journal of Fluids and Structures 20, 1085–1104.

Skop, R.A., Griffin, O.M., 1975. On a theory for the vortex-excited oscillations of flexible cylindrical structures. Journal of Sound and Vibration 41, 263–274.

Smith, J.D., 1962. An experimental study of the aeroelastic instability of rectangular cylinders. M.A. Sc. Thesis, University of British Columbia, Vancouver, Canada.

Vickery, B.J., Watkins, R.D., 1964. Flow-induced vibrations of cylindrical structures. In: Silvester, R. (Ed.), Proceedings 1st Australian Conference on Hydraulics and Fluid Mechanics. Pergamon, New York, pp. 213–241.

Williamson, C.H.K., Roshko, A., 1988. Vortex formation in the wake of an oscillating cylinder. Journal of Fluids and Structures 2, 355–381.